JOURNAL OF MATERIALS SCIENCE 24 (1989) 1219–1232

Deformation and transformation mechanisms of poly(vinylidene fluoride) (PVF_2)

T.-C. HSU, P.H. GEIL
Polymer Group, University of Illinois at Urbana-Champaign, 1304 West Green Street, Urbana, Illinois 61801, USA

The deformation process and the accompanying $\alpha \rightarrow \beta$ phase transformation of poly(vinylidene fluoride), drawn at 82 to 90 and 130° C, has been characterized by electron microscopy and X-ray and electron diffraction. Micronecking occurs at both draw temperatures, fibrils and mosaic blocks being drawn off the edges of the micronecks. The degree of phase transformation, at the same elongation, is dependent on the draw temperature; at 130° C the majority of the sample remains in the α phase at the natural draw ratio. The phase transformation at both draw temperatures accompanies the transformation from lamellar (block) structure to fibril.

1. Introduction

The increased interest in poly(vinylidene fluoride) (PVF_2) stemmed from the discoveries of its piezoelectric property by Kawai [1] in 1969 and its pyroelectric property by Bergman *et al.* [2] and Nakamura and Wada [3] in 1971. In addition to the extraordinary piezoelectric and pyroelectric properties, PVF_2 is also known for its complicated polymorphism. PVF_2 exists in at least four known crystalline structures; they are referred to as the α(Form II), β(Form I), γ(Form III) and δ (or α_p) (Form IV_p). A possible fifth crystalline modification has recently been suggested by Lovinger [4]. An excellent review article by Lovinger [5] summarized the structure, crystallization, morphology and properties of the four known crystalline structures of PVF_2. The α-phase is the most common structure of PVF_2 and is normally obtained by crystallization from the melt at moderate or high supercooling. The β-phase, being used extensively in piezoelectric and pyroelectric applications is technically the most important phase of PVF_2. The β-phase is routinely obtained by mechanical deformation of melt-crystallized films. Crystallization of the β-phase from the melt had been uncertain until the very recent success by Lovinger [6] who obtained the β-phase by epitaxial melt-solidification of PVF_2 on the (0 0 1) surface of freshly cleaved KBr. The γ-phase can be obtained by crystallization from the melt at high pressure as well as by crystallization from certain solutions. The δ-phase is formed by poling the α-phase at high electric fields; therefore, it is also known as the α_p phase.

Our interests in PVF_2 are on the transformation of melt-crystallized α-phase to β-phase during deformation. Previous studies showed that the drawing temperature determines the relative contents of α- and β-phase crystals in the drawn samples [7, 8]. At low draw temperatures, from about 80 to 100° C, transformation of α-phase to oriented β-phase readily occurs at draw ratios up to 400% engineering strain. At high drawing temperatures oriented α-phase is obtained up to these draw ratios, and it is only by drawing the material further that oriented β-phase becomes the dominant phase [8–10].

The results of Matsushige *et al.* [11] suggested that a heterogeneous stress distribution in the sample played a critically important role in the crystal transformation phenomenon during the $\alpha \rightarrow \beta$ transformation under tensile stresses. Based on their X-ray results, they observed the crystal transformation only for the samples where the deformation takes place in the cold-drawing temperature range (below ~ 130° C); the initiation of the phase transformation from α to β phase was detected at the deformation stage where necking was initiated at the centre of their tensile samples. Most of the studies of the α-phase to β-phase transformation during deformation have been by X-ray diffraction [7–11] and infrared spectroscopy [9, 12, 13]; only a few studies [12, 14, 15] of the stress-induced $\alpha \rightarrow \beta$ phase transformation have been done by electron microscopy and electron diffraction. We are interested in the morphological aspects of the $\alpha \rightarrow \beta$ phase transformation during deformation. The objective of this research is to characterize the deformation mechanisms of PVF_2 during deformation, in both thin films (~ 100 nm thick) and thick films (~ 1 mm thick). Because a phase transformation accompanies the deformation of PVF_2 and the resulting crystal structure is dependent on the temperature at which the deformation occurs [7–11], samples deformed at different temperatures were studied by electron microscopy and wide-(WAXD) and small-(SAXD) angle X-ray diffraction in order to understand better the morphological aspects of the $\alpha \rightarrow \beta$ tranformation during deformation.

2. Experimental details

2.1. Materials

Poly(vinylidene fluoride) (PVF_2) polymers manufactured by Pennwalt Corporation were the primary material used in the study. Kynar 821 resin was used

0022–2461/89 $03.00 + .12

for the morphology studies of thin films. Kynar 960 resin was used for the X-ray diffraction studies. Another resin, Solef (Soltex) fluoropolymer, which contains a lower percentage of head-to-head, tail-to-tail sequence, was used in X-ray studies as comparison.

Kynar 821 resin was chosen for the thin film morphology study because of its higher weight average molecular weight. It was our hope to obtain thin film samples with a thickness of the order of 100 nm, this being a desirable thickness that is both thin enough for electrons to penetrate and thick enough to be more than a few crystals thick. Thin films of high crystallinity (approaching 50%) and high strength are essential for studying the deformation behaviour of PVF_2 by electron microscopy. Kynar 960, which has a lower weight average molecular weight, was used for the X-ray studies because it was easily compression moulded into 1 mm thick films.

2.2. Sample preparation

2.2.1. Thick films

PVF_2 was melted at 220° C for 5 min, pressed for another 10 min at a pressure of 1200 psi (8.268 N/m^2) and then quenched in air. PVF_2 films of 1 mm thick were obtained. In some cases, compression moulded films were re-melted at 200 to 210° C for 4 min and then cooled again in air in order to obtain free surfaces for morphology studies.

2.2.2 Thin films

Thin films of PVF_2 were obtained by first solution casting from a fresh hot 0.3% (by weight) PVF_2/cyclohexanone solution on to carbon coated Mylar* films. The polymer–carbon–Mylar ensemble was then put into a nitrogen-purged oven at 200 to 210° C for 3 min to melt the PVF_2 polymer, and then allowed to cool in air to ambient temperature. A stretcher was used to retain the original length of the polymer–carbon–Mylar ensemble, i.e. to prevent shrinkage of the Mylar substrate during the remelt process.

2.3. Deformation

2.3.1. Thick films

Specimens of dumb-bell shape with a gauge length of 2.5 cm and a width of 0.8 cm were punched out by a laboratory test die. Deformed samples ranging from 27% to 510% deformation were obtained using a MTS model 820 tensile tester equipped with an oven chamber. Deformation was performed at a cross-head speed of 1 in. min^{-1} (~ 2.54 cm min^{-1}) and temperatures of 82 and 130° C. Deformation was performed about 2 min after samples were loaded in a pre-heated oven in order to allow the temperature of the oven to stabilize. As soon as the oven temperature reached the desired deformation temperatures, stress was applied. The heater was turned off immediately after the desired deformation ratio was reached. The drawn sample was slow cooled taut in the oven for 20 min. Stress–strain curves of the samples subjected to deformation were recorded simultaneously. A stretcher was used to secure the drawn sample before releasing from the MTS clamping jigs to prevent the retraction of the sample.

2.3.2. Thin films

Deformation of thin films was carried out by deforming the polymer–carbon–Mylar ensemble in a hand-operated stretcher in hot water at 90° C in order to achieve a high degree of localized deformation in the regions in which the carbon film cracked.

2.4. Experimental procedures

The permanganic acid etching technique used closely followed that described by Rybnikar and other workers [16–18] with only slight modifications. A solution of 1% (by weight) potassium permanganate ($KMnO_4$) in 85% phosphoric acid (H_3PO_4) was used as etchant. The powdered $KMnO_4$ was slowly added under agitation to the known volume of phosphoric acid. Samples were etched with fresh etchant in an ultrasonic bath for 40 min. Washing was carried out in an ultrasonic bath, using the following four steps: (1) 5 min in streaming water; (2) 15 min in 10 ml 30% solution of hydrogen peroxide (H_2O_2); (3) 5 min in running water; (4) 15 min in 10 ml acetone.

Wide-angle and small-angle X-ray diffraction patterns were obtained using a Philips (Norelco) X-ray diffraction generator equipped with a "Statton" camera. Cu$K\alpha$ radiation in transmission mode was used.

Electron microscopy was done using a Jeol JEM 100C transmission microscope (TEM) with observations being carried out at 100 kV. Kodak DEF X-ray film was used for some dark-field and diffraction studies.

3. Results

3.1. Deformation of thick films

3.1.1. Mechanical properties

Thick films of PVF_2, when deformation occurs at 82° C, undergo yielding, necking and strain hardening as the strain increases. Both types of samples we used have a local elongation at break of more than 500% at 82° C. "Solef" shows slightly better overall mechanical properties than Kynar 960 resin, as shown in the engineering stress–strain curves in Fig. 1. Previous studies [7, 8] have shown that the relative contents of α-phase and β-phase crystals in drawn samples vary with the temperature at which the deformation occurs. Fig. 2 shows representative engineering stress–strain curves of Kynar 960 resin deformed at 82 and 130° C. Not only is the stress level higher at 82° C, but there is a clear yield point maximum. At 130° C, on the other hand, the modulus is lower and only a slight indication of a yield maximum is seen. Both samples, Kynar and Solef at 82 and 130° C failed at approximately the same overall elongation.

In the sample drawn at 82° C, in addition to the whitening observed throughout the gauge length, a relatively sharp neck forms near the middle of the dumb-bell shaped sample and progresses towards each end; the initial local elongation in the neck region

*Trademark of E. I. du Pont de Nemours & Co., Inc.

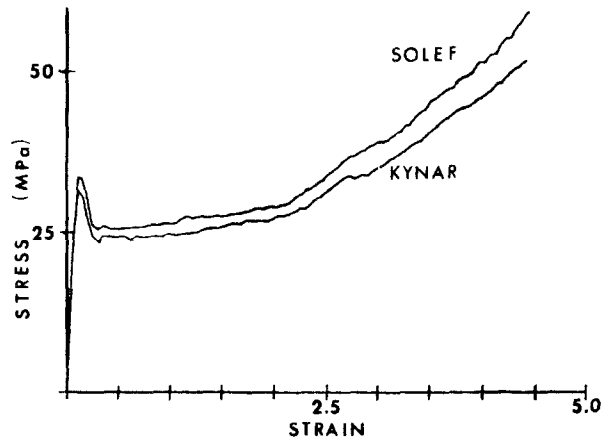

Figure 1 Stress–strain curves of two types of PCF_2 deformed at 82° C.

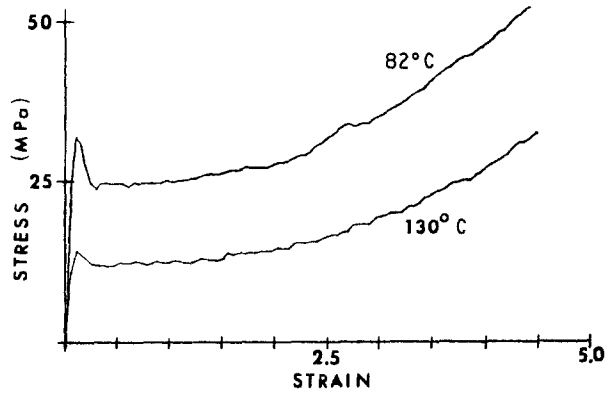

Figure 2 Stress–strain curves of PVF_2 deformed at 82 and 130° C.

is ~280%. When the neck reaches the end of the constant width portion of the dumb-bell the stress level increases, resulting in both further elongation of the already drawn material and the neck beginning to move into the wider portion of the dumb-bell. Failure finally occurs at a local elongation of more than 500%; samples studied were not drawn to failure. It is also noted that the elongations specified in the micrographs are those of the samples as shown. However, they are approximately the same as the actual elongation; following release from the clamping jigs the samples underwent negligible retraction.

In agreement with the literature for samples drawn at 140° C [11], in our first set of samples drawn at 130° C macroscopic necking did not occur. The sample elongated uniformly in the region of constant width to an elongation of ~310%, resulting in the development of an apparent neck at each end of the constant width portion. These necks then move into the wider regions of the dumb-bell, the narrow region undergoing further elongation. Failure again occurs at a local elongation greater than 500%. The above samples were slowly cooled from the melt. In subsequent sets of samples, slowly cooled or quenched from the melt, drawn at 130 or 140° C, a neck formed in the early stage of draw and, as in the case of the 82° C samples, travelled to both ends. The natural draw in the region between the necks was about the same as at 82° C, i.e. 280%; however, no whitening occurred.

Deformation by necking meant that it was impossible to obtain X-ray patterns from samples drawn between the yield strain and the natural draw ratio; the X-ray patterns would have to have been taken in the neck.

3.1.2. X-ray diffraction studies

WAXD of the initial necking region of the sample which necked at 130° C is shown in Fig. 3a. WAXD of PVF_2 (Kynar 960) deformed uniformly to various degrees between 310% and 510% at a temperature of 130° C are shown in Figs 3b to f. The WAXD of the necked sample (Fig. 3a) is essentially identical to that of the uniformly drawn sample (Fig. 3b) at the deformation ratio of about 300%. As shown in Figs 3a and b, a substantial amount of α-phase crystals still remain and are relatively well oriented even when the constant width portion is drawn to 310% elongation. A small amount of oriented β(1 1 0, 2 0 0, 0 2 0 and 2 0 1, 1 1 1 reflections) is also seen. As the strain in this region increases there is little further change in the pattern until one reaches ~510% elongation; (b), (c) and (d) are essentially identical. Three patterns (Figs 3d to f) are shown for 510% elongation, corresponding to increasing levels of engineering strain (i.e. 350%, 400% and 450% between the grips). In these patterns, despite the same local elongation, there is a change in the relative intensity of the α and β reflections. With increasing engineering strain the β reflections increase in intensity; the α reflections are nearly absent in Fig. 3f with only the 0 2 1 reflection still being clearly visible. It is noted that one might expect a contribution from γ reflections also, particularly for the lower degree of elongation (the γ phase readily undergoes a transition to β-phase when mechanically deformed [19]). However no evidence of an $l_\gamma = 1$ layer line is seen in any of the patterns, this layer line should be seen about halfway between the equator and the $l_\alpha = 1$ layer line if γ is present because the c axis for γ is about twice that for α and the (1 1 1) and (0 2 1) reflections of the γ-phase are strong.

WAXD taken from an area close to the neck region, of ~27% deformation, i.e. presumably a plastically deformed region, of the sample which necked when drawn at 130° C, showed three characteristic α diffraction rings with no orientation; the diffraction rings observed are identical to those obtained from the undrawn melt-crystallized films, indicating that the deformation may occur in the amorphous regions at this low deformation ratio.

The WAXD for the samples drawn at 82° C are shown in Fig. 4. Prior to necking, a small degree of plastic deformation occurs, i.e. a residual strain of up to at least 36% is observed in the regions which have whitened but have not yet undergone necking. The WAXD pattern, Fig. 4a, shows a slight degree of orientation, although probably not visible on the reproduction; the α diffraction rings are slightly more intense near the equator than near the meridian. As indicated, the lowest elongation following necking for which a patttern could be obtained was 280%. At this elongation there is only a small residue of α crystals; almost the entire sample has transformed to β. The α crystals that remain, while oriented with the molecular

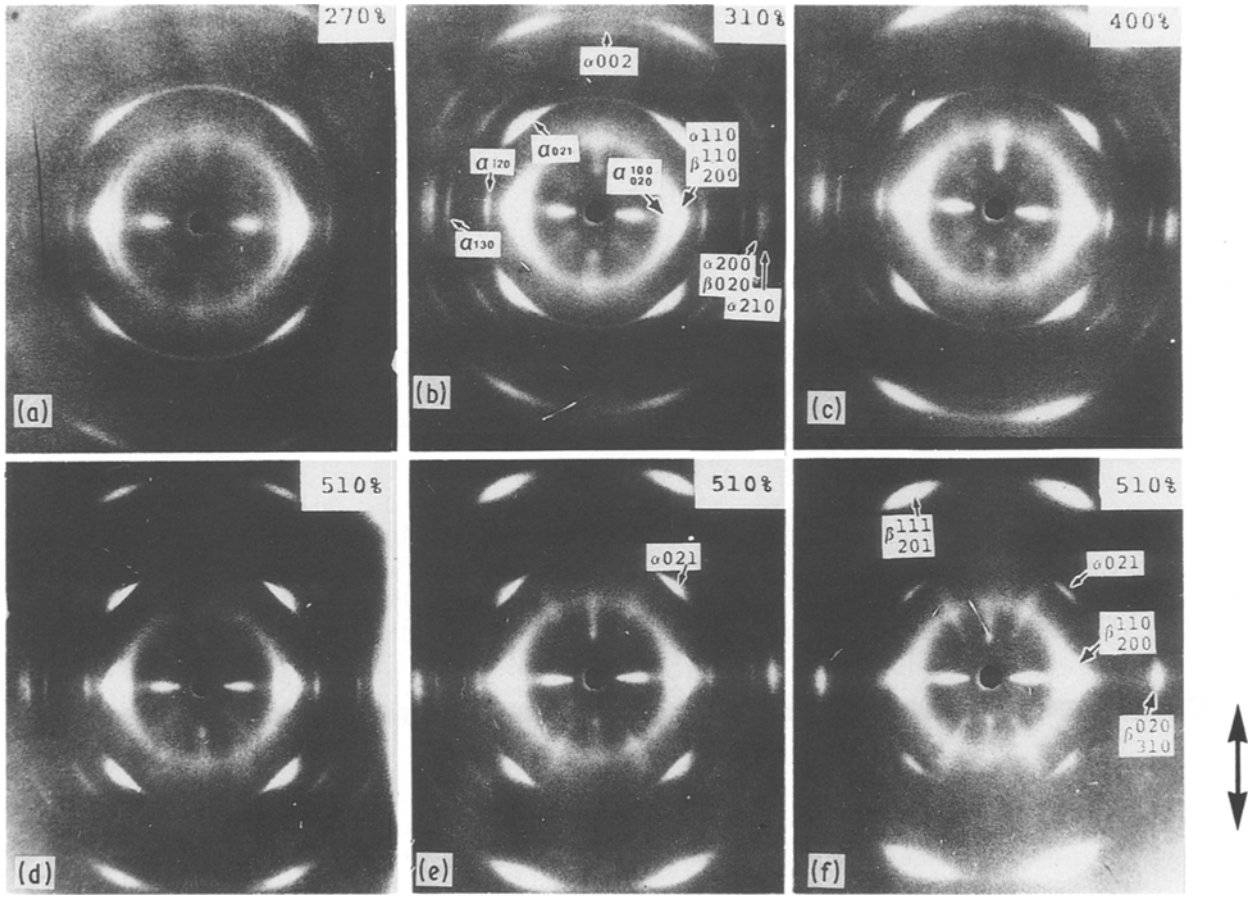

Figure 3 WAXD of PVF_2 deformed at 130° C, strain rate = 1 in. min^{-1} (2.54 cm min^{-1}). Local deformation ratios of the samples are (a) 270% (engineering strain 100%), (b) 310% (200%), (c) 400% (300%), (d) 510% (350%), (e) 510% (400%), (f) 510% (450%), respectively. All of the patterns are from the drawn regions of samples which did not neck when drawn except (a), which is from a subsequent set of "identical" samples, which did neck.

axes in the draw direction, have a much broader distribution of orientations than the relatively well-oriented β crystals. With increasing elongation of the drawn region, the α reflections decrease in intensity but remain broadly arced. By 440% elongation they are no longer visible on the negative. Over the entire characterizable elongation range, the β reflections remain sharply arced indicating a near constant degree of orientation. Presumably the increased elongation occurs as a result of molecular slippage and conversion of amorphous disoriented segments to aligned crystalline segments. Even though the samples decrease in thickness with increasing elongation, the intensity of the pattern in Fig. 4e is at least as strong or stronger than that in Fig. 4b. There appears to be a progressive increase in crystalline intensity per unit thickness.

In both sets of patterns (Figs 3 and 4) the amorphous halo is seen to have nearly uniform intensity around the ring, even at the highest elongation. The radial streaks within this ring are due to Bragg scattering of white radiation by the strong reflections in the same direction. The meridianal streaks are attributed to diffraction from the appropriate 0 0 l reflection; the actual reflections are weak or absent due to the high alignment and curvature of the sphere of reflection. The increase in degree of orientation with increasing elongation at 130° C can be seen from the narrowing of this streak; at 82° C the streak is already narrow at 280% elongation.

Figs 5 and 6 show the SAXD patterns of the samples drawn at 130 and 82°C, respectively. Periodicities are clearly observed in both sets of patterns, including the unoriented sample which had a spacing of 13 nm. In the samples drawn at 130° C the pattern (Fig. 5) consists of a short, broad (in the meridianal direction) line of discrete scattering and nearly circular central diffuse scattering. No second order of the discrete scattering can be seen even on the original negatives. At low degrees of elongation the maximum intensity in the lines is on the meridian. For the samples with 510% elongation, as in the case of the WAXD patterns, there is a change with increasing engineering strain; the discrete line scattering tends to separate into two spots, i.e. a four-point pattern develops. The separation of the spots increases with increasing engineering strain.

The long period spacings corresponding to the scattering intensity maxima were calculated using Bragg's law; the spacings are 12.9 nm for 310% and 400% elongation, measured along the draw direction to the centre of the line. At the 510% elongation, the axial spacing corresponding to the distance to the centre of the two spots decreases from 12.9 to 12.6 nm as the engineering strain increases. The radial spacing decreases even more, from 12.6 to 11.2 nm, as a result of the increasing separation of the spots.

At 82° C the SAXD patterns (Fig. 6) are considerably different at all elongations beyond yield. The

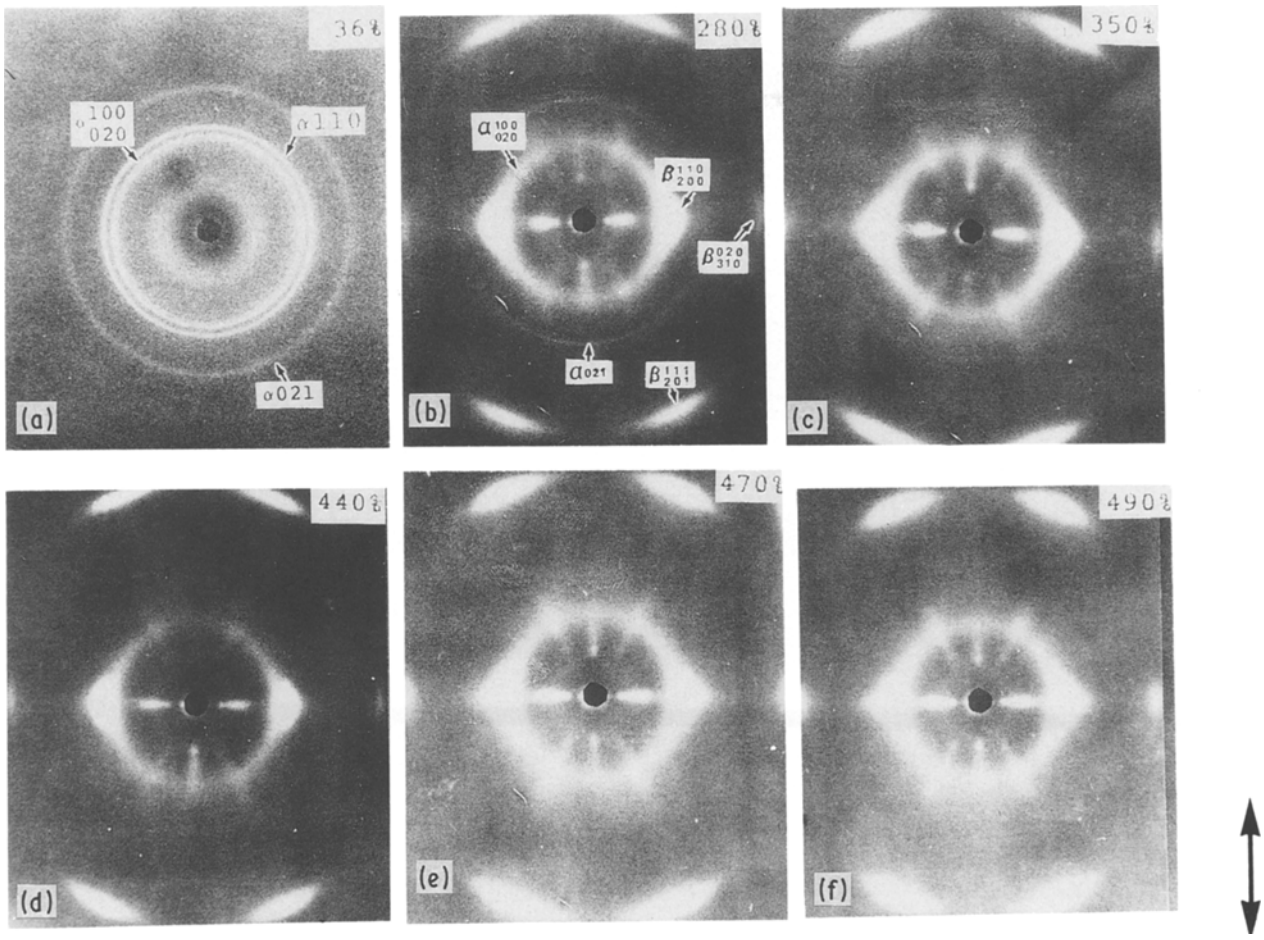

Figure 4 WAXD of PVF_2 deformed at 82° C, strain rate = 1 in. min (2.54 cm min^{-1}). Local deformation ratios (engineering strain) of the samples are (a) 36% (100%), (b) 280% (200%), (c) 350% (300%), (d) 440% (350%), (e) 470% (400%), (f) 490% (450%).

central diffuse scattering consists of very strong streaks elongated in the equatorial direction and the discrete scattering is a clear four-point pattern at all elongations. The streak tends to narrow and elongate with increasing elongation. The four-point pattern also becomes more distinct, the maxima tending to separate normal to the meridian and the pattern changing from two maxima on a line to a V-shape.

The long period spacing, 10.5 nm, measured along the draw direction to the centre of the line, is identical for all elongations. The radial spacings were 9.7 nm for 280% elongation decreasing to 9.0 nm for the highest elongation. The axial spacing, corresponding to the distance to the centre of the two spots is 10.1 nm for all elongations. Table I summarizes the calculated long-period spacings of samples investigated.

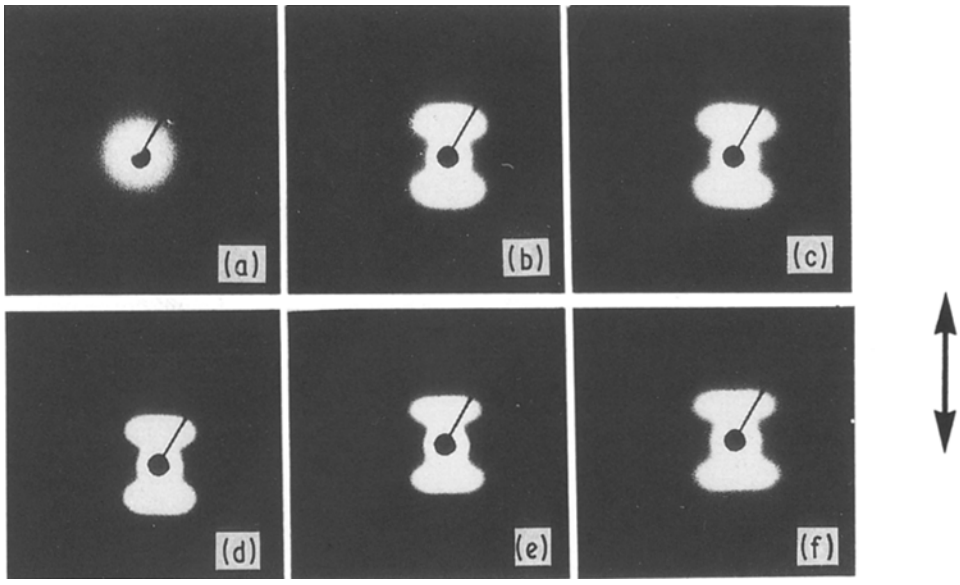

Figure 5 SAXD of PVF_2 deformed at 130° C. Local deformation ratios (engineering strain) are (a) as-melted undrawn sample, (b) 310% (200%), (c) 400% (300%), (d) 510% (350%), (e) 510% (400%), (f) 510%, (450%).

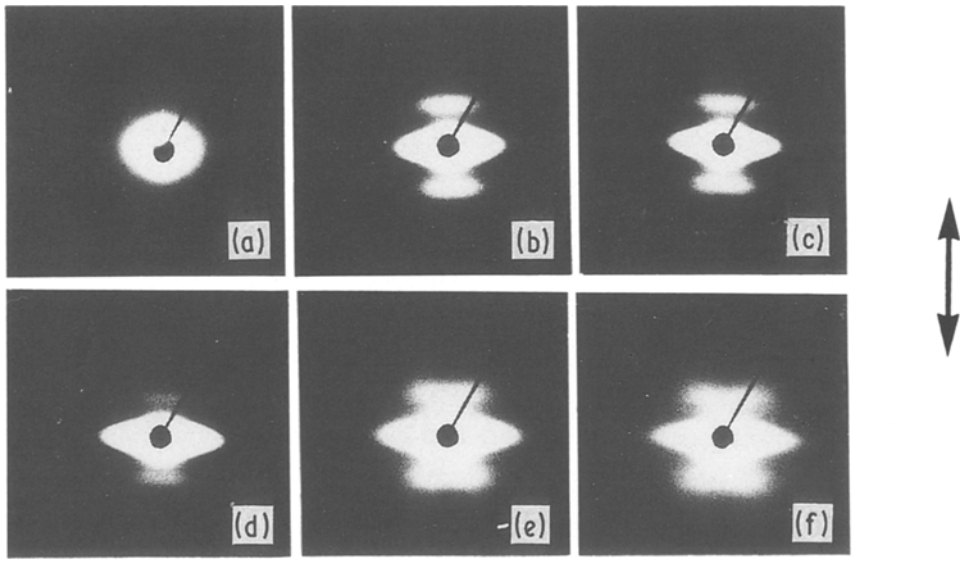

Figure 6 SAXD of PVF_2 deformed at 82° C. The local deformation ratios (engineering strain) are (a) 36% (100%), (b) 280% (200%), (c) 350% (300%) (d) 440% (350%), (e) 470% (400%), (f) 490% (450%).

3.1.3. Morphology of deformed thick films

Fig. 7 shows a replica of the typical free surface of melt-crystallized PVF_2 thick films. Although fine fibrils or lamellae are observed in some areas, the surface topography of PVF_2 thick films is, in general, obscured probably by oxidized and/or exuded low molecular weight material apparently developing during processing. The permanganic etching technique was used to study the morphology of PVF_2 thick films. Fig. 8 shows the permanganic-etched free surface of melt crystallized PVF_2 thick films. Despite the debris left over from the etching, the fibrillar or lamellar structure of PVF_2 is more clearly revealed. Plate-like structures, "A" in Fig. 8, are possibly catalysts or additives. Unfortunately, the washing process does not seem to clean the etched surfaces sufficiently; the debris is observed to be scattered non-randomly over the entire sample, with more in some areas than others.

Figs 9 and 10 show micrographs of surfaces of the central region of thick films deformed at 82° C and Fig. 11 of similar regions drawn at 130° C. Figs 12 and 13 show micrographs of the neck region at 82 and 130° C, respectively. Figs 9, 11, and 12 were etched after deformation whereas Fig. 10 and 13 were unetched. Fig. 9(a) shows a sample deformed 280%. X-ray data from this sample indicate that the sample contains mostly β-phase crystals (85%) and a few nearly randomly oriented α-phase crystals. Striations parallel to the draw direction are observed over almost the entire sample surface except for areas similar to "A", "B" and "C" in which portions of the original lamellae appear to remain. Presumably these regions are related to particular sectors or sections of the spherulites, but it was not possible to determine that relationship in these samples. A higher magnification picture of regions "A" and "B" is shown in Fig. 9b. The areas denoted "A" are regions in which the lamellae edges are oriented at a substantial angle to the draw direction. As in the case of the thin films (Fig. 17a), they appear to be broken up into blocks. In area "B" it is not clear whether the original lamellae or drawn fibrils are oriented parallel to the draw direction; the micrographs suggest, however, there is residual, relatively undrawn material (arrows in Fig. 9b) separated by fibrils. This is also the case for area "C" in Fig. 9a which is believed to consist of undrawn materials; regions similar to "C" are shown, at higher magnification, in Fig. 10a (also 280% deformation), as well as in regions "C" in Figs 12a and b. Although the detailed lamellar structures of the free surfaces of undrawn samples are easily observed on the surfaces of etched films, it is not clear whether etched or unetched surfaces better represent the deformation behaviour of deformed thick films.

Regions which are believed to consist of undrawn

TABLE I Calculated long period spacings of samples deformed at various deformation ratios at 130 and 82° C.

	Elongation (%) at 130° C						Elongation at 82° C				
	0%	310%	400%	510%	510%	510%	280%	350%	440%	470%	490%
d-spacing (nm) (centre)	13.0	12.9	12.9	12.9	12.6	12.6	10.5	10.5	10.5	10.5	10.5
d-spacing (nm) (radial)*	–	–	–	12.6	11.6	11.2	9.7	9.5	9.3	9.3	9.0
d-spacing (nm) (axial)†	–	–	–	–	–	–	10.1	10.1	10.1	10.1	10.1

*The spacings are measured along the diagonal direction to the centre of the two spots.
† The spacings are measured along the draw direction to the centre of the two spots.

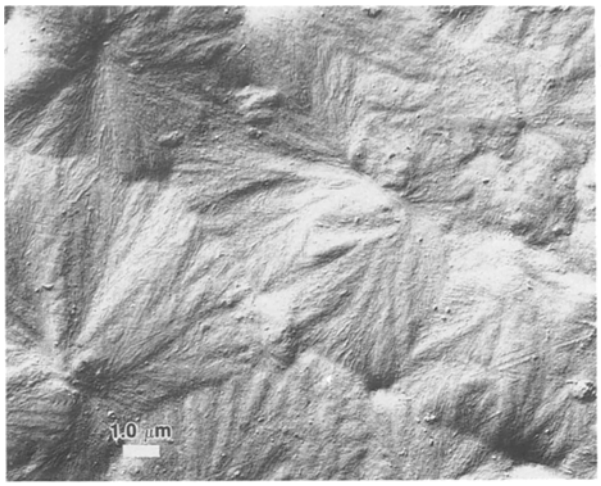

Figure 7 Replica of the free surface of a melt-crystallized PVF_2 thick film (unetched).

Figure 8 Replica of an etched free surface of melt-crystallized PVF_2 thick film showing lamellae structures. Plate-like structures A, are, suggested to be catalyst residues or additives. Arrows show the areas where the lamellae are lying at a shallow angle to the surface.

materials are denoted with arrows in Fig. 10a. The fibrils here, between the undrawn areas, often appear separated by elongated voids. Although we suggest the fibrils are drawn out from chunks of undrawn material in the regions with the arrows, it is also possible, in these unetched samples, that these chunks are low molecular weight residue lying on the surface; this is not the case in Figs 12a and b. In other regions of Fig. 10a, the striations are seen to be jagged, suggesting residual blocks of undrawn material from lamellae originally parallel to the draw direction.

The surface morphology of a sample deformed further at 82° C (locally 490%) is shown in Fig. 10b. "Catalyst residues", denoted "A" in this figure, are clearly observed; areas, denoted by arrows show that fibres are drawn off blocks. The heterogeneous nature of the deformation is again seen. It appears that some areas are deformed more than other areas in the sample. As in the case of the 280% deformation in Fig. 10a, the striations are jagged. In many regions, e.g. those marked with arrows, fibrils appear to be drawn out between blocks of residual "lamellae".

Figs 11a and b show the etched surfaces of samples deformed 310% and 510%, respectively, at 130° C. Area "A" in Fig. 11a shows numerous aggregates of degradation materials; there appears to be more of this material in samples deformed at 130° C compared to samples deformed at 82° C. X-ray data from this sample show that the sample contains mostly α-phase crystals and a few β-phase crystals. Striations parallel to the draw direction, similar to those observed in the samples deformed at 82° C, are observed. In a sample drawn 510% (Fig. 11b), most of the area consists of relatively smooth striations, presumably drawn fibrils. At the top of this figure one still sees the presence of broken up lamellae oriented more or less normal to the draw direction. Even at this high elongation and high draw temperature, the heterogeneous nature of the deformation is obvious.

As shown in Figs 9 to 11, surface of films drawn at 82° C are generally rougher than those drawn at 130° C, the undulations due to the striations are larger, while surfaces of films drawn at 130° C appear smoother with fibres oriented toward the draw direction. In addition, in general, more voids between fibres are observed in samples deformed at 82° C than in samples deformed at 130° C.

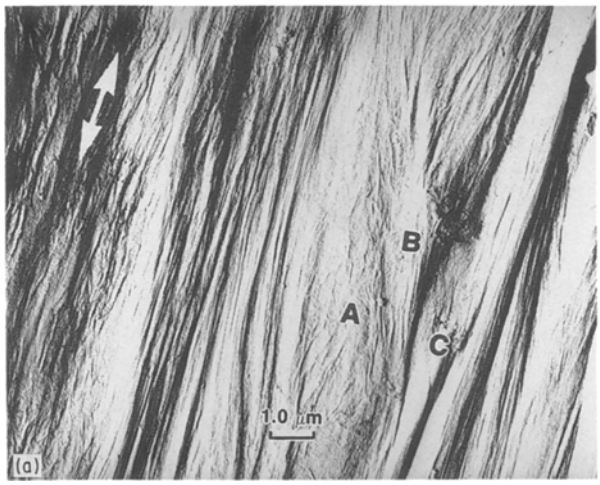

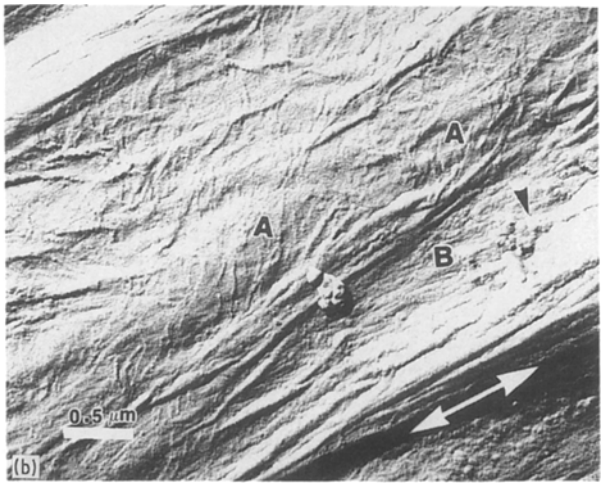

Figure 9 (a) Replica of the central, constant width region of an etched free surface deformed 280% at 82° C. A, lamellae oriented at an angle to the draw direction; B, lamellae oriented parallel to the draw direction; C, remaining undrawn material. (b) Higher magnification of (a); A, lamellae oriented at an angle to the draw direction, B, lamellae oriented parallel to the draw direction. Arrows show the undrawn materials.

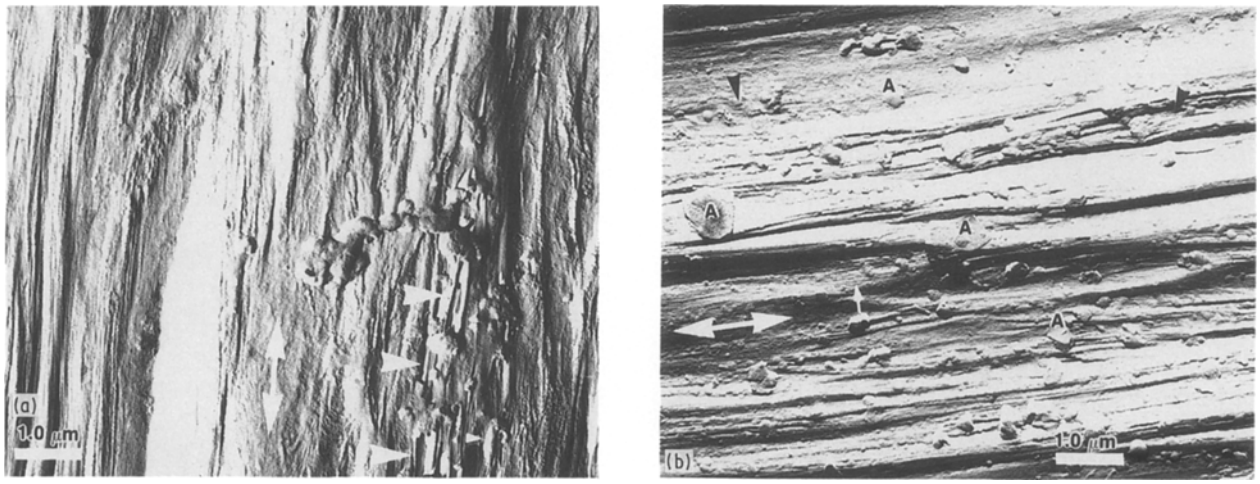

Figure 10 Replica of the central, constant width region of an unetched free surface deformed (a) 280% at 82° C, arrows show the formation of voids; (b) 490% at 82° C, showing "catalyst residues", A, and fibrils, arrows.

Figs 12a and b show the neck regions of etched free surfaces of samples deformed at 82° C; the local deformation cannot be defined. As shown in Fig. 12a, some areas, 'A", are highly deformed, whereas other areas, "B", show very little or no deformation. Areas denoted "C", at higher magnification in Fig. 12b, are regions where fibrils have formed and some undrawn materials remain. No obvious differences are observed in the neck regions of samples deformed at 82 or 130° C. Fig. 13 is the replica of the neck region of an unetched free surface of a sample deformed at 130° C showing fibres with diameters of the order of 10 nm being produced during deformation. The debris on this surface, we suggest, is due to the breaking up of exuded or degraded material on the original free surface.

In general, the micrographs of drawn thick films of PVF_2 are only partially satisfactory. Although, as indicated, it appears original fibrils or lamellae can be observed in some regions, even up to 510% deformation, the micrographs are admittedly not as clear as obtainable from other drawn polymers (e.g. polybutene (PB) and polyethylene (PE)). For this reason, we also examined the deformation of thin films of PVF_2.

3.2. Deformation of thin films

Thin films, originally solution cast and then melt crystallized, were studied by transmission microscopy after being drawn at 90° C across cracks in a carbon film on a grid. Fig. 14 shows the bright-field micrograph of PVF_2 before deformation. Electron diffraction indicates these films contain mostly α-phase crystals. The edges of the lamellae are considerably better resolved here than in the unetched bulk sample (Fig. 7). Most of the lamellae are on edge, making it difficult to determine their lateral width; it is believed they are lamellae, however, (i.e. have a significant lateral size) based on the etched surfaces of the bulk samples and the dark-field micrographs below of similar melt crystallized PVF_2 thin films. Three types of electron diffraction patterns are seen from these films. In the one type, which is most common, only nearly uniform $\alpha(1\,1\,0)$ and $\alpha(0\,2\,0)$ diffraction rings are seen. The other two are shown in Figs 15a and c with schematic diagrams in Figs 15b and d. In Fig. 15a one sees only $hk0$ reflections, whereas in Fig. 15c there are l index reflections as well; Fig. 15c resembles a poorly oriented fibre pattern. The dark-field micrograph in Fig. 16 was taken by placing the aperture on the $\alpha(0\,2\,0,\ 1\,1\,0,\ 0\,2\,1)$ rings of the type of pattern in

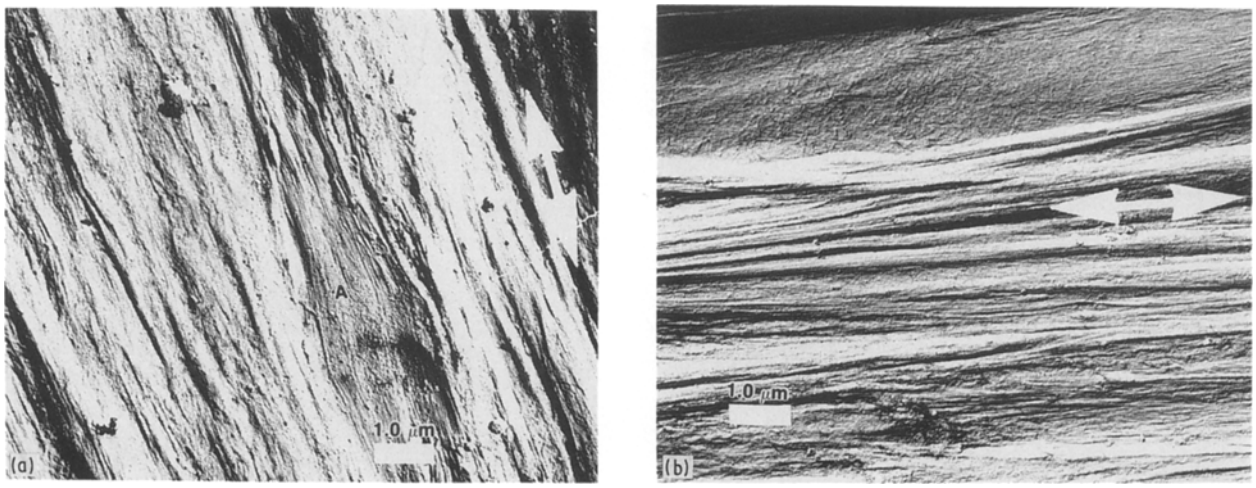

Figure 11 Replica of the central constant width region of an etched free surface deformed (a) 310% at 130° C showing fibril formation and degradation material due to etching; (b) 510% at 130° C showing fibrils and blocky structures.

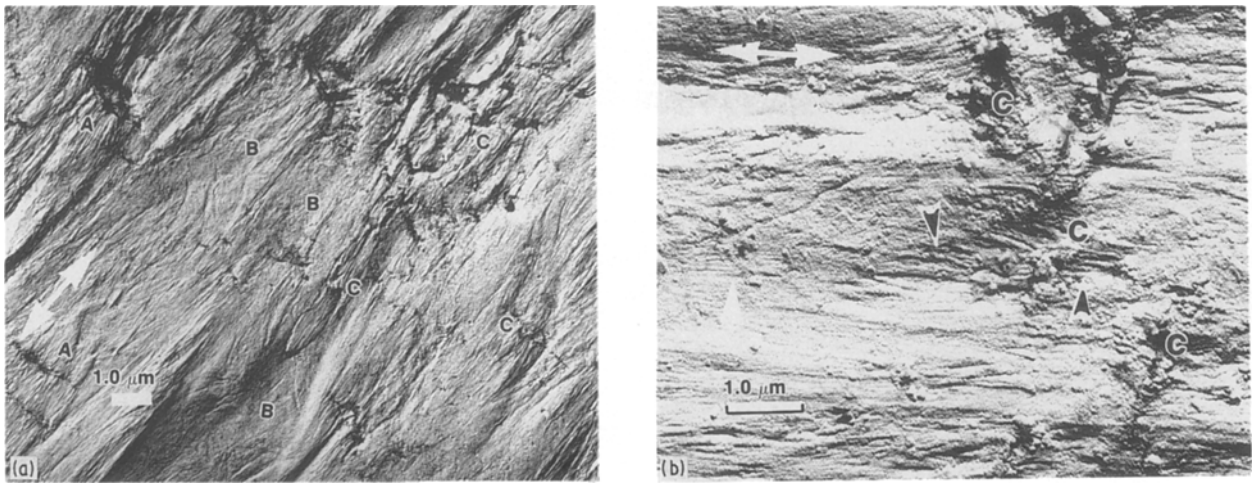

Figure 12 Replica of the neck region of an etched free surface deformed at 82° C. A, Areas showing fibres being formed; B, areas showing little or no deformation; C, remaining undrawn materials. (b) Higher magnification of the area "C" in (a), showing regions where undrawn materials, C, remain and fibrils, arrows, formed.

Fig. 15c. In Fig. 16 the areas designated "A" show lamellae oriented perpendicular to the sample surface, whereas the grey areas, labelled "B', are presumably lamellae parallel to the surface.

A bright-field micrograph of a melt-crystallized thin film deformed at 90° C in water is shown in Figs 17a and b. Similar to the deformation behaviour of PB proposed by Yang and Geil [20], deformation of PVF_2 thin films is dependent on the original lamellar orientation with respect to the draw direction. Blocky or mosaic structures are observed in the deformed region. Areas denoted "A" in Fig. 17a are the regions where lamellae were originally oriented perpendicular to the draw direction; areas denoted "B" are regions where lamellae were originally oriented parallel to the draw direction; areas denoted by arrows "C" show the inter-fibre links bridging the separated fibres in extremely highly deformed areas. A higher magnification of the region near "C", showing the inter-fibre links, mosaic blocks and residual lamellae is shown in Fig. 17b. Arrows "D" in Fig. 17a indicate the edges of the carbon substrate. One can calculate the deformation ratio simply by dividing the total width of the crack by the sum of the distances from both edges of the carbon substrate to the undeformed regions. The draw ratio of the deformed region shown in Fig. 17a is calculated to be 550%.

Electron diffraction patterns from the deformed regions show the samples contain a mixture of α-phase and β-phase crystals. As shown in Fig. 17a (1), which was obtained from an area corresponding to the bright-field micrograph shown here, only a few diffraction rings are visible in the deformed region, as compared to those observed in the undeformed region (Figs 15a and c), this may be due to the very small crystals in the deformed region and less crystalline material (thinner sample) contributing to the diffraction pattern. A second type of electron diffraction pattern observed from deformed thin films, as shown in Fig. 17a (2), shows a different orientation for the α diffraction arcs with respect to the draw direction. Both electron diffraction patterns from the deformed regions, however, show relatively broadly arced α diffraction rings, indicating a substantial amount of the residual α-phase crystals are poorly oriented with respect to the draw direction, and well-oriented β-phase crystals, presumably transformed at the expense of the well-oriented α-phase crystals. Thus, compared to the WAXD pattern of thick film deformed 490% at 82° C (Fig. 4f), in which the pattern indicated

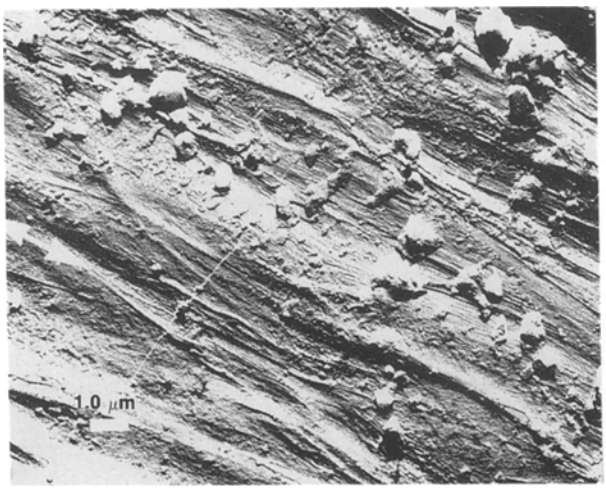

Figure 13 Replica of the neck region of an unetched free surface deformed at 130° C.

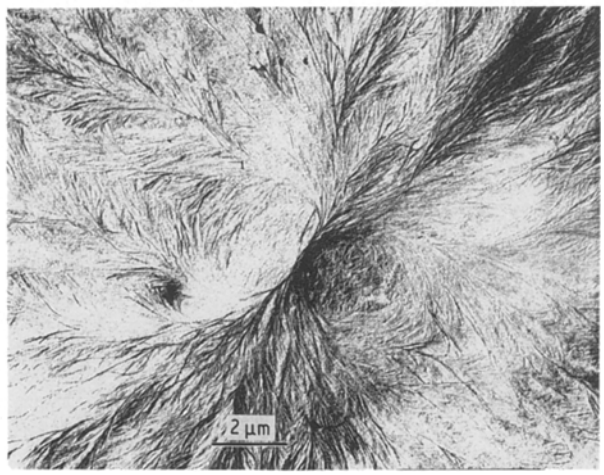

Figure 14 Bright-field micrograph of a melt-crystallized PVF_2 thin film containing mostly α-phase crystals.

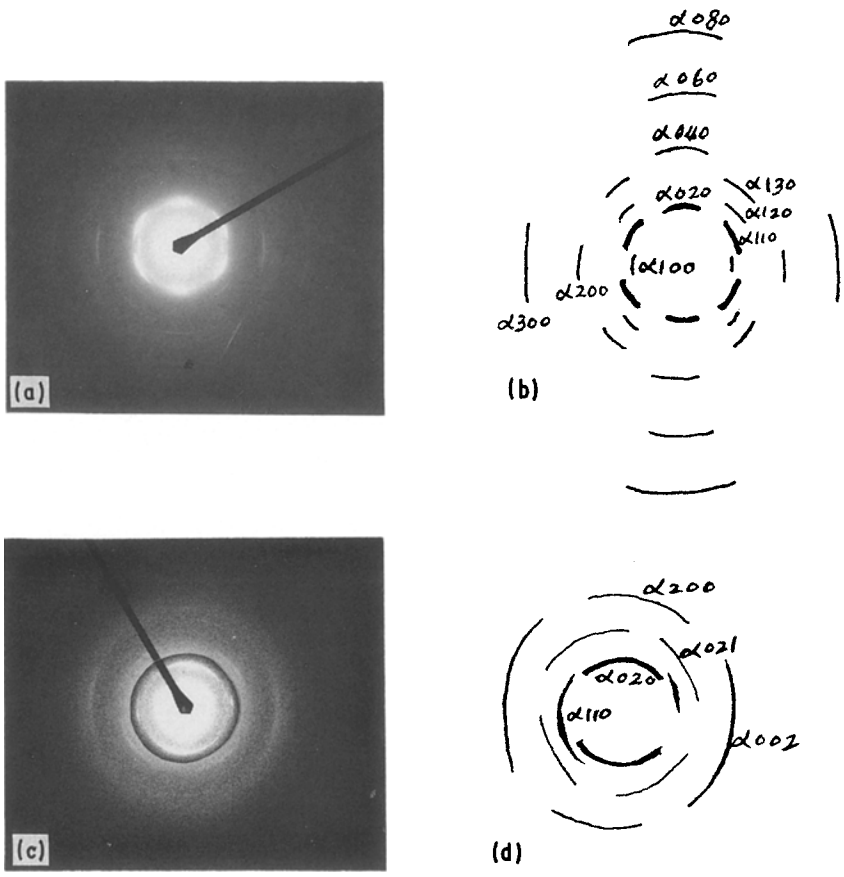

Figure 15 (a) to (d) Electron diffraction patterns of the melt-crystallized thin films. (a) ED pattern obtained from an area where the lamellae are presumably lying parallel to the sample surface, (b) schematic diagram of ED pattern in (a), (c) ED pattern obtained from an area where the lamellae are perpendicular to the sample surface, (d) schematic diagram of ED pattern in (c).

a "complete" transformation from α-phase to β-phase at 490% deformation, i.e. no α-phase crystals were observed, the electron diffraction pattern of the deformed thin film shows that a substantial amount of poorly oriented α-phase crystals remain in the deformed region even at a deformation ratio as high as 550%.

Fig. 18 shows a dark-field micrograph of a deformed PVF_2 thin film. The dark field was taken by placing the aperture at the equatorial position of the multiple rings, α(1 0 0, 0 2 0, 1 1 0) and β(1 1 0, 2 0 0). Although crystals are observed in the undeformed regions, no crystals are visible in the deformed regions. This is believed due to the extremely small crystal size in the deformed regions with insufficient crystalline material in a given crystal to give rise to enough scattering to be detectable by the photographic film used.

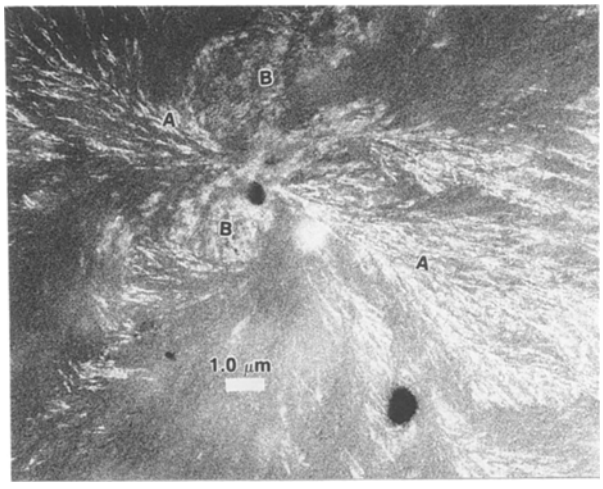

Figure 16 Dark-field micrograph of a spherulite in a melt-crystallized PVF_2 thin film. The black areas are holes in the film. A, Image of crystals lying almost perpendicular to the sample surface; B, image of crystals lying parallel to the sample surface.

4. Discussion

4.1. Effect of deformation temperature on thick films

Anaysis of the above experimental results allows us to conclude that there is a substantial difference in the mechanism of deformation and in the structure of PVF_2 deformed at 82° C (cold drawing) and at 130° C (hot drawing). Our results generally agree with the earlier findings by Kosmynin *et al.* [15].

Consider first the samples drawn at 80 to 90° C, as shown by our WAXD and SAXD results in Figs 4 and 6, in which a macroscopic neck is formed 280% drawn samples consist of mostly well-oriented but highly defective and small β-phase crystals (~85%), a small amount (~15%) of presumably original, nearly unoriented α-phase crystals, and considerable numbers of longitudinal voids. The presence of the voids is indicated by the streak in the direction of the equator in SAXD patterns, as shown in Fig. 6 and the whitening of the sample. The transformation from the α-phase to β-phase crystals occurs primarily in those regions in which the crystals are aligned in the draw direction, i.e. the fibrils seen in the electron micrographs. The essentially unoriented α-phase crystals, a residue still being seen at 350% elongation, i.e. after the neck has already reached the ends of the sample and the drawn material is being stretched further, presumably belong to the blocks observed on the micrographs of these samples.

Kosmynin *et al.* [15] have suggested that when,

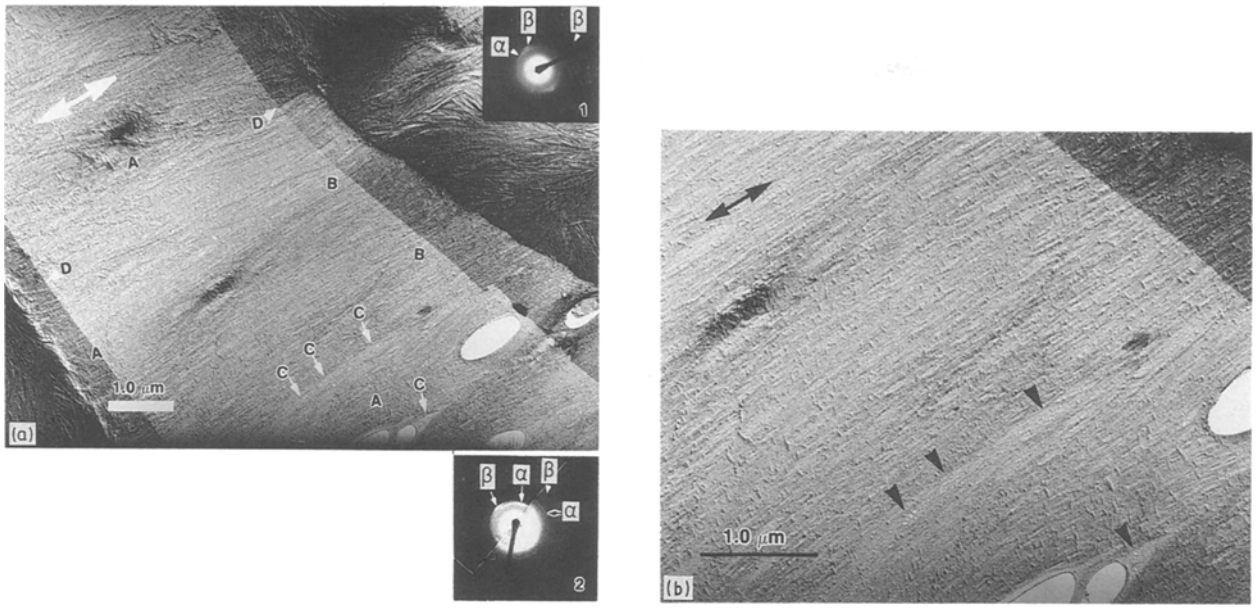

Figure 17 Bright-field micrograph of a deformed thin film. A, Areas where lamellae were originally oriented perpendicular to the draw direction; B, lamellae were originally oriented parallel to the draw direction; C, inter-fibre links bridging the fibres; D, edges of the carbon substrates. Inserts: (1) ED pattern obtained from the area as shown, (2) ED pattern from a different area. (b) Higher magnification of (a) showing the inter-fibre links spanning splits in the drawn film.

during deformation of PVF_2, a certain critical stress is reached, rotation around C–C bonds becomes possible and in these segments of the polymer chain, in addition to the orientation of the segments in the direction of stretching, the polymer undergoes a change from the coiled α-phase conformation to the planar zigzag β-phase conformation. In other segments stressed below the critical stress, the original structure remains and therefore, in a neck, in addition to well-oriented β-phase crystals, there are unoriented α-phase crystals. Based on our WAXD studies and the thin-film electron microscopy and electron diffraction studies discussed below, we suggest the critical stress for samples drawn at 82° C is that required to unfold the molecules and form fibrils, i.e. the transformation occurs at the time of fibril formation.

The WAXD pattern from the sample drawn 36% (Fig. 4a) shows only a slight degree of orientation, with no evidence for β reflections. Presumably most of the permanent deformation has occurred between the lamellae resulting in the opening of voids; the observed WAXD orientation may be due to molecular tilt within the lamellae.

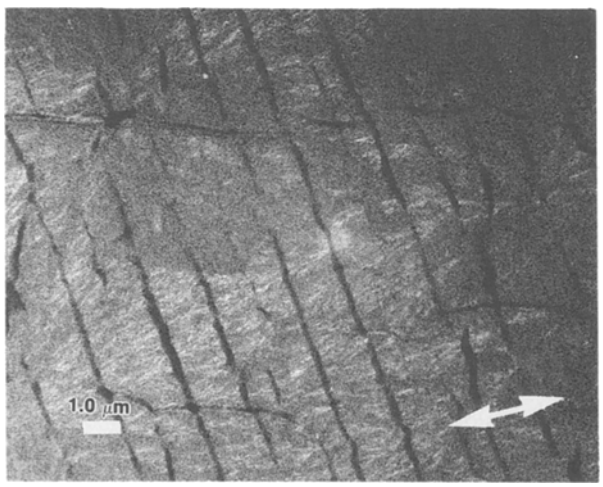

Figure 18 Dark-field micrograph of a deformed PVF_2 thin film showing α-phase crystals in the undeformed regions.

Following necking, an entirely new SAXD spacing is found, ~10.5 nm along the draw direction, as compared to the 13.0 nm spacing for the original lamellae, as well as a diffuse "streak". Clearly a new set of crystals has been formed, accompanied by the transformation from α to β. The streak is attributed to voids elongated in the draw direction, i.e. between the fibrils. Whether they are due to elongation of the voids observed by SAXD and sample whitening before necking or are a new set of voids, cannot be determined. The discrete diffraction is in the form of a four-point pattern in which the lateral distance between the pairs of points appears to increase with increasing draw ratio. The morphological origin of a four-point SAXD pattern in "fully drawn" samples is not yet clear. Somewhat similar, but inverted, V-shaped patterns have been reported in the necking region of polyethylene, the spacings being related to the original lamellae [21]. In this case the pattern and its change with deformation can be related to the original lamellae retaining a periodicity at an angle to the draw direction. However, in fully drawn polyethylene a line pattern is observed with a new spacing that is dependent on the draw temperature. This model of tilted lamellae cannot apply directly to our system; the V, if present, is in the opposite direction, the angle between the lamellae and the draw direction is of the order of 70° and decreases with degree of draw, and the spacing is not related to the original spacing. It may be that wavy lamellae are present, in the sense described by Bonart [22], or that there is a knob and neck packing of crystallites, as described by Statton [23], but we have no EM evidence for either model.

We suggest that at the lamellar level, some lamellae may tilt along the draw direction while others break into lamellar blocks, depending upon the original

orientation of the lamellae with respect to the stress direction [20, 24]. The transformation from α to β crystals occurs, similar to the behaviour in the thin films discussed below, as soon as the fibrils are pulled out from the lamellae or blocks.

At the hot-drawing temperature, 130° C, necking was not observed in our first set of samples, although the literature [11] suggests it occurs at 130° C. In subsequent sets of samples, although with the same thermal history, draw rate, etc., necking did occur at 130° C and also at 140° C (at which temperature the literature claims necking does not occur), preventing us from obtaining X-ray patterns from samples of degrees of deformation between 27% and 270%. The presence or absence of necking seems to make no major difference in the X-ray observation; as shown in Figs 3a and b, one with necking and the other without, the patterns of samples drawn to about 300% are essentially identical. In both one finds predominantly oriented α reflection with only a small amount of slightly better oriented β crystals. Because these samples are already fibrillar, as observed in the electron microscope, clearly the α crystals present have realigned or been formed during fibril formation.

Previous studies, based on thermodynamic arguments, suggest that the chain mobility in the crystal lattice during hot drawing is so high that it allows the original crystals to be oriented towards the draw direction during deformation without transformation [15, 24]. Chain slippage in the lamellae or blocks occurs readily such that large stresses cannot be applied by taut tie molecules in the amorphous regions. As shown in Figs 3a or b, at about 300% deformation the sample contains mostly oriented α-phase crystals and a small number of β-phase crystals. In contrast to deformation at 82° C, it is not clear from the SAXD patterns whether or not a new set of crystals is formed when the fibrils are formed; the spacing of the line pattern is essentially the same as the original lamellar periodicity. This could be by chance due to the particular deformation temperature chosen.

With increasing elongation there is a gradual conversion of oriented α to oriented β phase crystals. Presumably after fibril formation stresses are transferred from crystal to crystal, the critical stress, as defined by Kosmynin *et al.* [15], can be reached in the α crystal, and transformation occurs. Even at the maximum elongation achieved, however, a residue of oriented α crystals remain. Even though the local elongation of the three patterns shown in Figs 3d to f remains the same, the decrease in α diffraction with total stress on the sample can be seen, particularly by the decrease in intensity of the $\alpha(0\,2\,1)$ quadrant reflections; these three patterns correspond to increasing engineering strain as the neck moves into the wider portion of the dumb-bell shaped sample. The significantly smaller SAXD diffuse scattering in these samples than in those drawn at 82° C, in agreement with the lack of whitening, indicates few or no voids are formed. The four-point pattern at high elongation (and high engineering strain) may again be related either to wavy lamellae or a knob and neck packing of crystallites.

In general, the morphology of drawn PVF_2 films indicates a heterogeneous deformation at both 82 and 130° C. Blocks of undrawn materials are observed even at 510% deformation. Samples deformed at 82° C show a greater amount of the undrawn blocks throughout the samples at the various deformation ratios investigated, as compared to samples deformed at 130° C. Judging from the shadows of the striations observed in the replica of the drawn samples, it appears that more of the fibres formed by deforming the samples at 82° C are separated from each other due to the formation of voids between fibres, than in the case of the fibres formed by deforming the sample at 130° C; at 130° C the fibres are coherent.

The etching technique used, although somewhat helpful in revealing the lamellar structure of bulk films, unfortunately creates an artefact on the etched surface as well. Nonetheless, the morphology of the deformed thick films shows clearly the blocky structures and fibrils, similar to those observed in the deformed thin films.

4.2. Deformation and transformation in thin films

As shown in Fig. 14, it is difficult to determine whether the basic morphological unit in these α-spherulites are lamellae, laths or ribbons, or fibrils. If lamellae or ribbons, nearly all of them are on edge. Based on the grey areas in the dark-field micrograph (Fig. 16) and a few areas of the bright-field replicas (arrows in Fig. 8) in which there is some lateral size of the morphological units, they appear to be lamellae. It is not clear, however, why these lamellae are predominantly nearly perpendicular to the surface on the free surfaces of both thick (Figs 7 and 8) and thin films.

The electron diffraction patterns and corresponding diagrams in Figs 15a to d represent two types of preferred crystal orientation within the spherulites. The nearly complete $\alpha(1\,1\,0)$ and $\alpha(0\,2\,0)$ rings seen in the majority of the cases are presumably the result of either too large a selected-area aperture relative to the size of domains of common orientation within a spherulite and/or superposition of varying orientation through the thickness of the thin films. The patterns in Fig. 15a and the schematic diagram, Fig. 15b are single crystal-like in that only $h\,k\,0$ reflections are seen. Inasmuch as the radial (growth) direction of the α spherulites has been reported to be the b-axis [25], presumably the vertical axis of the pattern in Fig. 15a corresponds to the radius of the spherulite. The lamellae in this region of the spherulite must have been parallel to the surface, corresponding to the grey areas in Fig. 16 (areas "B"). The arcing will be due to a distribution of growth directions within the selected area.

The patterns in Fig. 15c and the schematic diagram, Fig. 15d, on the other hand, presumably come from areas in which the lamellae are perpendicular to the surface. Other than for the two $(1\,1\,0)$ sharp arcs, of which the presence and location vary from pattern to pattern, the pattern resembles that from a poorly oriented fibre; the spherulite radius and the lamellae are presumably oriented in the vertical direction. Two

features need pointing out, the orientation of the lamellae giving rise to the majority of the pattern and the origin of the (1 1 0) reflections that are seen. On the equator of the "fibre" pattern one sees both (0 2 0) and (2 0 0) reflections, i.e. the growth directions of the lamellae represented would appear to both lie in the film (as represented by the bright line in the dark-field micrographs) and perpendicular to the film. In addition the lack of a (1 1 0) reflection on the equator of the "fibre" pattern suggests that only these two lamellar orientations are present. The (1 1 0) reflections that are seen are presumably not related to the remainder of the reflections; in particular the line connecting the two 1 1 0 reflections is at an angle of about 70° to the equator of the pattern.

As in the case of the thick films drawn at 82°, a phase transformation from α-phase to β-phase is observed when the thin film is deformed at 90° C. The detailed mechanism of deformation is suggested to depend on the original orientation of the lamellae with respect to the draw direction. In the regions denoted "A" in Fig. 17a, where the lamellae were originally perpendicular (molecules parallel) to the draw direction, deformation starts in the amorphous regions between the lamellae; the lamellae are pulled apart as the stress increases. Inhomogeneities in the deformation result in breaking up of the lamellae into blocks and shear of the blocks. The molecular chains within the blocks may shear along their axes, unfolding from the edges will result in a decrease in lateral size of the blocks and molecular extension in the draw direction. Deformation propagates by pulling molecules out of the blocks, resulting in their separation and decrease in lateral size.

In the regions denoted "B" in Fig. 17a, the lamellae were originally parallel (molecules perpendicular) to the stress direction; deformation is proposed to start first within the lamellae because the stress will primarily be supported by the crystals. Deformation will occur in the inter-lamellar amorphous regions which are in parallel with the lamellae, as the crystalline lamellae begin to elongate through molecular tilt and rotation. Defects present initially or as a result of deformation result in breaking up of the lamellae into smaller crystalline blocks; their separation results in further elongation of the inter-lamellar regions. Micronecks between the blocks propagate by pulling molecules out of the blocks by chain unfolding and reorientation to form microfibrils, with the blocks becoming smaller. When the blocks are destroyed at extremely high deformation ratios, and the molecules within the blocks have been oriented parallel to the stress direction, inter-fibre separation occurs, as shown in Fig. 17b. The molecular chain axis, which was originally perpendicular to the stress direction in the crystals, would have been rotated through a 90° angle, and become parallel to the stress direction. Further deformation results in breakage of the inter-fibre links, fibre slippage and, finally, failure of the sample.

The electron diffraction patterns from the deformed regions, similar to those shown in the inserts of Fig. 17a, indicate the molecular axes in the β-phase crystals are well oriented toward the stress direction, whereas the remaining α-phase crystals show a distribution of molecular orientation; the α(0 2 0) is a broad arc with a maximum just off the equator in the pattern (1) and at about 45° to the equator in the other pattern (2) taken from a different area of a deformed sample. These patterns presumably correspond to regions in which the lamellae originally had different orientations with respect to the draw direction; the remaining α reflections correspond to a distribution of molecular orientations still remaining in these regions. The β pattern always indicates a high degree of orientation nearly parallel to the draw direction, regardless of the original α orientation. We suggest that the β-phase crystals form as the molecules are unfolded from the blocks and aligned in the fibrils. In contrast to the literature [8, 11], which suggested the α crystals are first oriented in the draw direction and then transformed, it is clear that the β crystals can be formed from α crystals with various orientations relative to the draw direction; i.e. the transformation occurs during the micronecking process as the molecules are unfolded form the original blocks and aligned in the fibrils.

In the case of polybutene, which morphologically undergoes a similar type of deformation in thin films [26], the majority of the crystalline segments transformed from the original tetragonal crystals into the stable hexagonal crystals while still incorporated in the original lamellae, i.e. during tilt and slip of molecules within the blocks. According to the electron diffraction patterns from regions deformed to various degrees, the only residual tetragonal crystalline regions were those in which the original lamellae were nearly perpendicular (molecules parallel) to the draw direction, i.e. those regions in which the lamellae become separated. Thus, in contrast to the transformation behaviour in polybutene thin films, in which the phase transformation occurs while the crystalline segments are still incorporated in the original lamellae during tilt and slip of molecules within the blocks [26], in PVF_2 the transformation during deformation at 90° C appears to occur only during or after the molecules are stripped off the blocks and fibrils are formed. Hence, we can conclude that while the deformation mechanisms of PVF_2 thin films depend upon the original orientation of lamellae with respect to the draw direction, as in the case of polybutene, the transformation from α to β crystals in the thin films of PVF_2 and presumably in the thick films as well, when drawn at 80 to 90° C, regardless of the orientation of the original molecular axes of the α-phase crystals, occurs as soon as molecules are pulled into fibrils. Based on the WAXD results, however, at 130° C deformation temperature the α crystals can be aligned or reformed in the fibrils before the transformation occurs.

5. Conclusions

1. Oriented PVF_2, fully drawn at either 82 to 90 or 130° C, consists predominantly of fibrils on the order of 10 nm diameter. As shown by whitening of the sample and a high intensity of void scattering in small-angle

X-ray diffraction, the fibrils are less coherent when drawn at the lower temperatures, i.e, there are numerous elongated voids in the "cold drawn" samples. In films of commercially significant thickness necking occurred in most of our samples at both draw temperatures, to an elongation of $\sim 300\%$, followed by further elongation to $\sim 500\%$ before failure.

2. The phase transformation, as followed by X-ray and electron (in thin films) diffraction, from anti-polar α to the polar β phase is strongly dependent on the temperatures at which the deformation occurs. At the natural draw ratio, i.e. about 300%, the transformation is essentially complete in the "cold drawn" samples whereas at 130° C a majority of the sample is still α phase and it is only near failure that the transformation approaches completion.

3. The morphological mechanism of deformation in thin films drawn at 90° C has been characterized by bright- and dark-field electron microscopy. Micronecking occurs, with fibrils and mosaic blocks being drawn off of the edge of the microneck (similar blocks have only been observed in the deformation of polybutylene, in most polymers fibrils alone are seen in drawn regions). With increasing deformation of the drawn regions molecules are "unfolded" from the blocks and transformed to fibrillar material. In contrast to polybutylene, where a crystal–crystal phase transformation can occur in the blocks when under stress, in PVF_2 the phase transformation occurs only during fibril formation.

4. In thick films, observed by electron microscopy utilizing replicas, a similar type of deformation appears to occur at both draw temperatures, i.e. fibrils and mosaic blocks are present in the drawn regions. Again, when cold drawn, the phase transformation occurs during fibril formation. At 130° C, however, considerable α-phase remains in samples which are essentially completely fibrillar. Whether these are remainders (small blocks) of the original crystals or newly formed α crystals cannot be determined.

References

1. H. KAWAI, *Jpn J. Appl. Phys.* **8** (1969) 975.
2. J. G. BERGMAN Jr, J. H. McFEE and G. R. CRANE, *Appl. Phys. Lett.* **18** (1971) 203.
3. K. NAKAMURA and Y. WADA, *J. Polym. Sci. A-2* **9** (1971) 161.
4. A. J. LOVINGER, *Macromol.* **15** (1982) 40.
5. *Idem*, in "Developments in Crystalline Polymers", edited by D. C. Bassett (Applied Science, London, 1982) pp. 195–273.
6. *Idem, Polymer* **22** (1981) 412.
7. J. B. LANDO, H. G. OLF and A. PETERLIN, *J. Polym. Sci. A-1* **4** (1966) 941.
8. B. P. KOSMYNIN, Ye. L. GAL'PERIN and D. Ya. TSVANKIN, *Polym. Sci. USSR* **12** (1970) 1418.
9. J. C. McGRATH and I. M. WARD, *Polymer* **21** (1980) 855.
10. A. RICHARDSON, P. S. HOPE and I. M. WARD, *J. Polym. Sci. Polym. Phys. Edn* **21** (1983) 2525.
11. K. MATSUSHIGE, K. NAGATA, S. IMADA and T. TAKEMURA, *Polymer* **21** (1980) 1391.
12. D. C. YANG and E. L. THOMAS, *J. Mater. Sci. Lett.* **3** (1984) 929.
13. H. W. SIESLER, *J. Polym. Sci. Polym. Phys. Edn* **23** (1985) 2413.
14. Ye. L. GAL'PERIN, Y. V. STROGALIN and M. P. MLENIK, *Vysokomol. Soed.* **7** (1965) 933.
15. B. P. KOSMYNIN, Ye. L. GAL'PERIN and D. Ya. TSVANKIN, *ibid.* **A12** (1970) 1254.
16. F. RYBNIKAR, *J. Appl. Polym. Sci.* **30** (1985) 1949.
17. R. H. OLLEY, A. M. HODGE and D. C. BASSETT, *J. Polym. Sci. Polym. Phys. Edn* **17** (1979) 627.
18. K.L. NAYLOO and P. J. PHILLIPS, *ibid.* **21** (1983) 2011.
19. S. WEINHOLD, M. H. LITT and J. B. LANDO, *Macromol.* **13** (1980) 1178.
20. Y. C. YANG and P. H. GEIL, *Makromol. Chem.* **186** (1985) 1961.
21. H. HENDUS, "Chemie und Technologie der Kunststoffe", Vol. 4, Aufl. (1963).
22. V. R. BONART, *Kolloid. Z. Polymere B.211* **H.1-2** (1966) 14.
23. P. F. DISMORE and W. O. STATTON, *J. Polym. Sci.* **B2** (1964) 1113.
24. A. PETERLIN, *J. Polym. Sci. C* **18** (1967) 123.
25. A. J. LOVINGER, *J. Polym. Sci. Polym. Phys. Edn* **18** (1980) 793.
26. T. C. HSU and P. H. GEIL, (1989) to be published.

Received 10 February
and accepted 13 June 1988